Self-potential, soil CO_2 flux, and temperature on Masaya volcano, Nicaragua

J. L. Lewicki[1,2], C. Connor[1], K. St-Amand[3], J. Stix[4], and W. Spinner[1]

Short title: SELF-POTENTIAL ON MASAYA VOLCANO

[1]Department of Geology, University of South Florida, Tampa, Florida, USA.

[2]now at Lawrence Berkeley National Laboratory, Berkeley, California, USA.

[3]formerly at Département de Géologie, Université de Montréal, Montréal, Quebec, Canada.

[4]Department of Earth and Planetary Sciences, McGill University, Montréal, Canada.

Abstract.

We investigate the spatial relationship between self-potential (SP), soil CO_2 flux, and temperature and the mechanisms that produce SP anomalies on the flanks of Masaya volcano, Nicaragua. We measured SP, soil CO_2 fluxes (<1 to 5.0 x 10^4 g $m^{-2}d^{-1}$), and temperatures (26 to 80^{o}C) within an area surrounding a normal fault, adjacent to Comalito cinder cone (2002-2003). These variables are well spatially correlated. Wavelengths of SP anomalies are $\leq$100 m, and high horizontal SP gradients flank the region of elevated flux and temperature. Carbon isotopic compositions of soil CO_2 (δ^{13}C = -3.3 to -1.1$^o/_{oo}$) indicate a deep gas origin. Given the presence of a deep water table (100 to 150 m), high gas flow rates, and subsurface temperatures above liquid boiling points, we suggest that rapid fluid disruption is primarily responsible for positive SP anomalies here. Concurrent measurement of SP, soil CO_2 flux, and temperature may be a useful tool to monitor intrusive activity.

Introduction

Self-potential (SP) anomalies have been observed within many volcanic and hydrothermal regions, and SP variations have been linked to changes in volcanic activity and hydrothermal fluid flow [e.g., *Corwin and Hoover*, 1979; *Fitterman and Corwin*, 1982; *Massenet and Pham*, 1985; *Zlotnicki and LeMouel*, 1988; *Hashimoto and Tanaka*, 1995; *Zlotnicki et al.*, 2003]. Monitoring these anomalies on active volcanoes may therefore be a valuable tool to forecast eruptions and understand interaction between magmatic and groundwater systems. SP anomalies have commonly been attributed to electrokinetic (EK) processes involving transport of charge contained in the electrical diffuse layer at the pore surface by electrolyte solution flow [e.g., *Anderson and Johnson*, 1976; *Massenet and Pham*, 1985; *Revil et al.*, 1999; *Ishido and Pritchett*, 1999]. However, *Johnston et al.* [2001] proposed that rapid fluid disruption (RFD), a process whereby charge separation can be produced by rapid disruption or vaporization of liquid water by high heat and/or gas flow, may be primarily responsible for SP anomalies observed in many volcanic areas. Unlike EK potentials, which are commonly produced by capillary flow of aqueous solutions, RFD may produce SP anomalies in thermal areas far above the groundwater table as charge is carried by water droplet and/or vapor flow [*Johnston et al.*, 2001].

The integration of soil gas flux and chemistry, temperature, SP, and hydrologic data should elucidate the mechanism(s) that produce SP anomalies on active volcanoes and therefore improve the use of SP in volcano monitoring. We present soil CO_2 flux,

temperature, and SP data measured concurrently on the flanks of Masaya volcano, Nicaragua (Figure 1) and show that these data are well spatially correlated. We suggest that RFD may be the primary mechanism to produce SP anomalies at Masaya and that tracking the relative temporal changes in SP and soil CO_2 flux may serve as an important volcano monitoring tool.

Figure 1.

Methods

The study area, located adjacent to Comalito cinder cone (Figure 1) is characterized by fumarolic steam emissions along an inferred normal fault. Evidence of high gas and heat flow [*St-Amand*, 1998; *Pérez et al.*, 2000] and basic understanding of the shallow ground water system [*Sandberg and Connor*, 2002] make this an excellent location to investigate correlation of gas flux and SP. In August, 2002, 209 measurements of soil CO_2 flux and temperature were made at uneven spacing within a 7175 m^2 area adjacent to Comalito (Figures 1 and 2). In February-March, 2003, 469 measurements of CO_2 flux, temperature, and SP were made at one-m spacing along four traverses that crossed perpendicular to an inferred normal fault located within the same study area. Twenty-three soil gas samples were collected at 75 cm depth from within or near this area in March, 1997 and February, 1998.

Figure 2.

CO_2 flux was measured using the accumulation chamber (AC) method [e.g., *Chiodini et al.*, 1996] with a LI-COR LI-800 infrared gas analyzer. Measurement accuracy and repeatability of the AC method are -12.5% [*Evans et al.*, 2001] and ± 10% [*Chiodini et al.*, 1998], respectively. Soil temperature was measured at 20 cm depth by

thermocouple. SP was measured using two $Cu/CuSO_4$ non-polarizing electrodes, an insulated Cu cable, and a digital multimeter. SP measurements along each traverse are referenced to the first station at the southwest end of each traverse. Carbon isotope ratios of soil CO_2 were measured by dual-inlet gas-isotope mass spectrometry (measurement error = $\pm$ 0.4$^o/_{oo}$). Carbon-13 data are reported as δ^{13}C, the deviation, in parts per thousand ($^o/_{oo}$) of the $^{13}C/^{12}C$ ratio in the sample from that of the Peedee belemnite (PDB) reference standard.

Results

CO_2 fluxes and temperatures measured in 2002 ranged from 27 to 4.2 x 10^4 g $m^{-2}d^{-1}$ (Figure 2) and 30 to 80^{o}C, respectively. Fluxes are log-normally distributed into two overlapping populations [*Sinclair*, 1974]. Log fluxes and soil temperatures are well positively correlated (correlation coefficient, C = 0.81). An interpolated (Krigging method) image map (Figure 2) shows that elevated fluxes are distributed along linear trends sub-parallel to the fault. Multiplying the mean of the Krigged CO_2 flux data (2750 g $m^{-2}d^{-1}$) by the sampling area (7175 m^2), total CO_2 discharge from this area is $\sim$20 tons day^{-1}. Carbon-13 values of soil CO_2 range from -3.3 to -1.1$^o/_{oo}$.

CO_2 fluxes and temperatures measured in 2003 along transects C1-C4 ranged from <1 to 5.0 x 10^4 g $m^{-2}d^{-1}$ and 26 to 79^{o}C, respectively (Figure 3). Wavelengths of SP anomalies are $\leq$ 100 m. High horizontal SP gradients flank the region of elevated flux and temperature (e.g., 26 mV m^{-1} on SW side of transect C1). Log CO_2 flux and soil temperature are well positively correlated (C = 0.84, 0.86, 0.86, and 0.92 for

Figure 3.

transects C1, C2, C3, and C4, respectively). Self-potential is well positively correlated with soil temperature (C = 0.81, 0.84, 0.79, and 0.81 for transects C1, C2, C3, and C4, respectively) and moderately correlated with flux (C = 0.67, 0.71, 0.59, and 0.70 for transects C1, C2, C3, and C4, respectively).

Discussion and Conclusions

Soil CO_2 fluxes measured on the flanks of Masaya are among the highest reported for volcanoes worldwide, including Cerro Negro, Nicaragua [*Salazar et al.*, 2001], Solfatara, Italy [*Chiodini et al.*, 2001], and Mammoth Mountain, USA [*Farrar et al.*, 1995]. Observed spatial trends in soil CO_2 fluxes and temperatures and good correlation between these variables are indicative of advective transport of heat and CO_2 with steam along a highly permeable fault zone.

The age of Comalito is unknown; however, we measured elevated soil CO_2 fluxes and temperatures, up to 1.4 x 10^4 g $m^{-2}d^{-1}$ and 78^{o}C, respectively, on the cone rim in February, 2003. The source of gas and heat at our study site may therefore be a cooling intrusion at relatively shallow depth, related to Comalito. Also, δ^{13}C values indicate that soil CO_2 is likely a mixture of CO_2 from mantle (-9 to -4 $^o/_{oo}$; *Pineau and Javoy* [1983]) and marine carbonate (0 $\pm$ 4 $^o/_{oo}$; *Ohomoto and Rye* [1979]) sources.

Observed correlation of SP with both soil CO_2 flux and temperature suggests that electrical current density is proportional to fluid flow at the ground surface where outflow conditions exist. Higher correlation of SP with soil temperature than CO_2 flux may be attributed to the dominant mechanisms of gas and heat transport. Advective

transport of CO_2 through highly permeable fractures is likely the dominant mode of CO_2 flow here [e.g., *Xu and Pruess*, 2001]; surface CO_2 fluxes will therefore be relatively highly spatially variable. Heat transport is likely a combination of advection through fractures and conduction through the surrounding media. We therefore expect soil temperature to be less spatially variable. Because SP is a potential field measurement, it is less sensitive to small scale heterogeneities in the porous fractured media, and spatial trends should more closely resemble those of temperature.

Transient electromagnetic soundings [*Sandberg and Connor*, 2002] indicate depth to the water table at the study site is 100 to 150 m and high resistivities ($\sim$1000 ohm-m) in the geologic section above the groundwater table. This is consistent with shallow (<5 m) terrain conductivity measurements made at the study site in 2003, which yield resistivities of 400 to 1500 ohm-m. To evaluate whether EK effects from near-surface fluid flow can account for observed SP anomalies, we calculated the SP anomaly arising from a uniformly polarized thin vertical sheet in a homogeneous subsurface with a top at 100 m depth (i.e., minimum depth to the water table) [*Babu*, 2003]. The wavelength of the calculated SP anomaly is >>100 m and the horizontal gradient of the anomaly is much less than those observed along transects C1-C4 (Figure 3). Polarization must be shallow (<10 m) to produce the high horizontal SP gradients observed at the study site. It is therefore unlikely that observed SP anomalies are due in large part to EK effects, as proposed by *Johnston et al.* [2001] for similar observations near active vents on Kilauea. Given the presence of mechanisms to produce RFD (i.e., subsurface temperatures above liquid boiling points, high gas flow rates), a thick unsaturated zone, and relatively

high resistivities, it is likely that SP anomalies are mainly produced by RFD, although some contribution from EK effects due to shallow two-phase flow [e.g., *Antraygues and Aubert*, 1993] may also be occurring.

The concurrent temporal measurement of SP, soil temperature, and CO_2 flux may be used to monitor intrusive activity. Injection of magma to relatively shallow crustal levels should be accompanied by increased magmatic heat and gas flow. As the heat and gas interact with the shallow groundwater system, RFD could occur. In this case, we expect that a positive SP anomaly will be formed at the surface in conjunction with elevated CO_2 discharge. Soil temperature anomalies may be slower to follow, due to the combined effects of conductive and advective heat transport. As magma continues to rise to near-surface levels, a groundwater dry-out zone will form around the intrusion above which we predict increased surface temperatures and magmatic gas flow rates to occur in the absence of SP anomalies. Integration of these geochemical and geophysical methods should be further investigated as a volcano monitoring tool.

Acknowledgments.

We acknowledge NASA grant NA-11318 for partial funding of this work. We thank M. J. S. Johnston, an anonymous reviewer, and G. E. Hilley for constructive review of the manuscript and L. Connor, G.E. Hilley, E. Mayorga-Caldera, W. Sanford, and W. Strauch for helpful assistance in the field.

References

Anderson, L. A., and G. R. Johnson, Application of the self-potential method to geothermal exploration in Long Valley, California, *J. Geophys. Res.*, *81*, 1527–1532, 1976.

Antraygues, P., and M. Aubert, Self-potential generated by two-phase flow in a porous medium: experimental study and volcanological applications, *J. Geophys. Res.*, *98*, 22,273–22,281, 1993.

Babu, R., Relationship of gravity, magnetic, and self-potential anomalies and their application to mineral exploration, *Geophysics*, *68*, 181–184, 2003.

Chiodini, G., F. Frondini, and B. Raco, Diffuse emission of CO_2 from the Fossa crater, Vulcano Island (Italy), *Bull. Volcanol.*, *58*, 41–50, 1996.

Chiodini, G., G. R. Cioni, M. Guidi, B. Raco, and L. Marini, Soil CO_2 flux measurements in volcanic and geothermal areas, *Appl. Geochem.*, *13*, 543–552, 1998.

Chiodini, G., C. Cardellini, F. Frondini, D. Granieri, L. Marini, and G. Ventura, CO_2 degassing and energy release at Solfatara Volcano, Campi Flegrei, Italy, *J. Geophys. Res.*, *106*, 16,213–16,221, 2001.

Corwin, R. F., and D. B. Hoover, The self-potential method in geothermal exploration, *Geophysics*, *44*, 226–245, 1979.

Evans, W. C., M. L. Sorey, B. M. Kennedy, D. A. Stonestrom, J. D. Rogie, and D. L. Shuster, High CO_2 emissions through porous media: transport mechanisms and implications for flux measurement and fractionation, *Chem. Geol.*, *177*, 15–29, 2001.

Farrar, C. D., M. L. Sorey, W. C. Evans, J. F. Howle, B. D. Kerr, B. M. Kennedy, Y. King,

and J. R. Southon, Forest-killing diffuse CO_2 emission at Mammoth Mountain as a sign of magmatic unrest, *Nature*, *376*, 675–678, 1995.

Fitterman, D. V., and R. F. Corwin, Inversion of self-potential data from the Cerro-Prieto geothermal field, Mexico, *Geophysics*, *47*, 938–945, 1982.

Hashimoto, T., and Y. Tanaka, A large self-potential anomaly on Unzen volcano, Shimabara peninsula, Kyushu island, Japan, *Geophys. Res. Lett.*, *22*, 191–194, 1995.

Ishido, T., and J. W. Pritchett, Numerical simulation of electrokinetic potentials associated with subsurface fluid flow, *J. Geophys. Res.*, *104*, 15,247–15,259, 1999.

Johnston, M. J. S., J. D. Byerlee, and D. Lockner, Rapid fluid disruption: A source for self-potential anomalies on volcanoes, *J. Geophys. Res.*, *106*, 4327–4335, 2001.

Massenet, F., and V. N. Pham, Mapping and surveillance of active fissure zones on a volcano by the self-potential method, Etna, Sicily, *J. Volcanol. Geotherm. Res.*, *24*, 315–338, 1985.

Ohomoto, H., and R. O. Rye, Isotopes of sulfur and carbon, in *Geochemistry of hydrothermal ore deposits*, edited by H. L. Barnes, Wiley, New York, 1979.

Pérez, N., J. Salazar, A. Saballos, J. Álvarez, F. Segura, P. Hernández, and K. Notsu, Diffuse degassing of CO_2 from Masaya caldera, Central America, *Eos Trans. AGU, Fall Meet. Suppl.*, *81*, 2000.

Pineau, F., and M. Javoy, Carbon isotopes and concentrations in mid-oceanic ridge basalts, *Earth Planet. Sci. Lett.*, *62*, 239–257, 1983.

Revil, A., H. Schwaeger, L. M. C. III, and P. D. Manhardt, Streaming potential in porous

media 2. Theory and application to geothermal systems, *J. Geophys. Res.*, *104*, 20,033–20,048, 1999.

Salazar, J. M., P. A. Hernández, N. M. Pérez, G. Melián, J. Álvarez, F. Segura, and K. Notsu, Diffuse emission of carbon dioxide from Cerro Negro volcano, Nicaragua, Central America, *Geophys. Res. Lett.*, *22*, 4275–4278, 2001.

Sandberg, S. K., and C. Connor, Geophysical investigation of the hydrogeologic structure and magma at Masaya Volcano, Nicaragua, *Eos Trans. AGU, Fall Meet. Suppl.*, *83*, 2002.

Sinclair, A. J., Selection of threshold values in geochemical data using probability graphs, *J. Geochem. Exploration*, *3*, 129–149, 1974.

St-Amand, K., The distribution and origin of radon, CO_2, and SO_2 gases and multifractal behavior of SO_2 at Masaya volcano, Nicaragua, Master's thesis, Université de Montréal, 1998.

Xu, T., and K. Pruess, On fluid flow and mineral alteration in fractured caprock of magmatic hydrothermal systems, *J. Geophys. Res.*, *106*, 2121–2138, 2001.

Zlotnicki, J., and J. L. LeMouel, Possible electrokinetic origin of large magnetic variations at La Fournaise volcano, *Nature*, *343*, 633–636, 1988.

Zlotnicki, J., Y. Sasai, P. Yvetot, Y. Nishida, M. Uyeshima, F. Fauquet, H. Utada, Y. Takahashi, and G. Donnadieu, Resistivity and self-potential changes associated with volcanic activity: The July 8, 2000 Miyake-jima eruption (Japan), *Earth Planet. Sci. Lett.*, *205*, 139–154, 2003.

J. L. Lewicki, Lawrence Berkeley National Laboratory, Earth Science Division, 1 Cyclotron Rd., MS 90-1116, Berkeley, California, 94707 USA

C. Connor, Department of Geology, 4202 E. Fowler Ave., SCA 528, University of South Florida, Tampa, Florida, 33620 USA

K. St-Amand, Labo S.M. 1471, Lionel Boulet Boulevard, Varennes, Quebec, J3X 1P7, Canada

J. Stix, Department of Earth and Planetary Sciences, McGill University, 3450 University St., Montréal, Quebec, H3A 2A7, Canada

W. Spinner, Department of Geology, 4202 E. Fowler Ave., SCA 528, University of South Florida, Tampa, Florida, 33620 USA

Received _____

This manuscript was prepared with AGU's LaTeX macros v5, with the extension package 'AGU^{++}' by P. W. Daly, version 1.6b from 1999/08/19.

Figure Captions

Figure 1. Areal photograph showing study site location adjacent to Comalito cinder cone on the flanks of Masaya volcano. Inset (A) shows locations of inferred normal fault (dashed line), 2002 measurement locations (dots), and transects C1-C4.

Figure 2. Interpolated (Krigging method) image map of log CO_2 flux measured adjacent to Comalito cinder cone. White dashed line and dots show locations of inferred normal fault and soil CO_2 flux and temperature measurements (temperature data not shown), respectively. Also shown are locations of transects C1-C4.

Figure 3. Plots of log CO_2 flux and soil temperature versus distance along transects (a) C1, (c) C2, (e) C3, and (g) C4 (see Figure 2). Dots and pluses are log CO_2 flux and soil temperature, respectively. Plots of SP versus distance along transects (b) C1, (d) C2, (f) C3, and (h) C4.

Figures

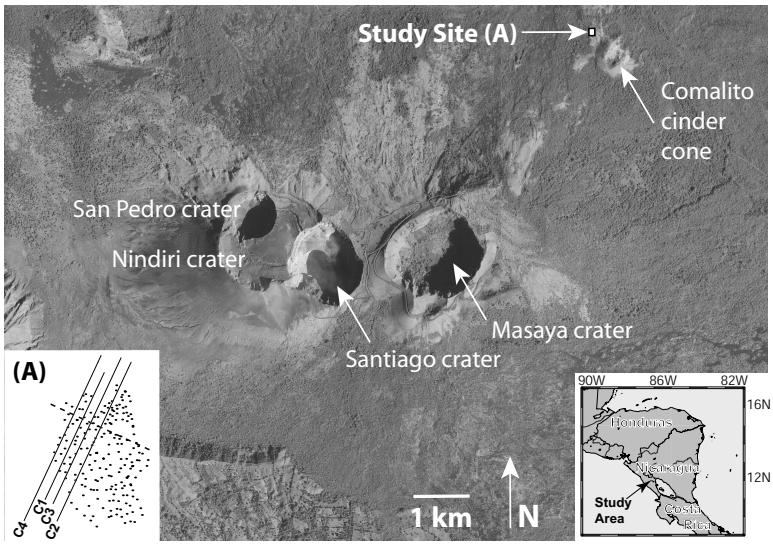

Figure 1. Areal photograph showing study site location adjacent to Comalito cinder cone on the flanks of Masaya volcano. Inset (A) shows locations of inferred normal fault (dashed line), 2002 measurement locations (dots), and transects C1-C4.

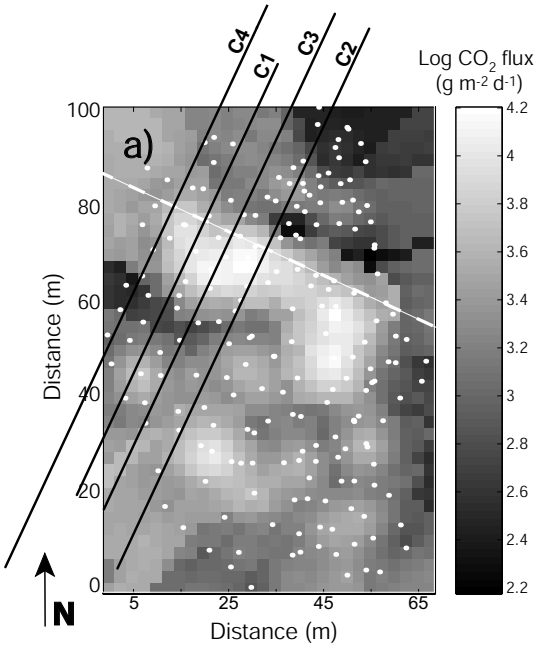

Figure 2. Interpolated (Krigging method) image map of log CO_2 flux measured adjacent to Comalito cinder cone. White dashed line and dots show locations of inferred normal fault and soil CO_2 flux and temperature measurements (temperature data not shown), respectively. Also shown are locations of transects C1-C4.

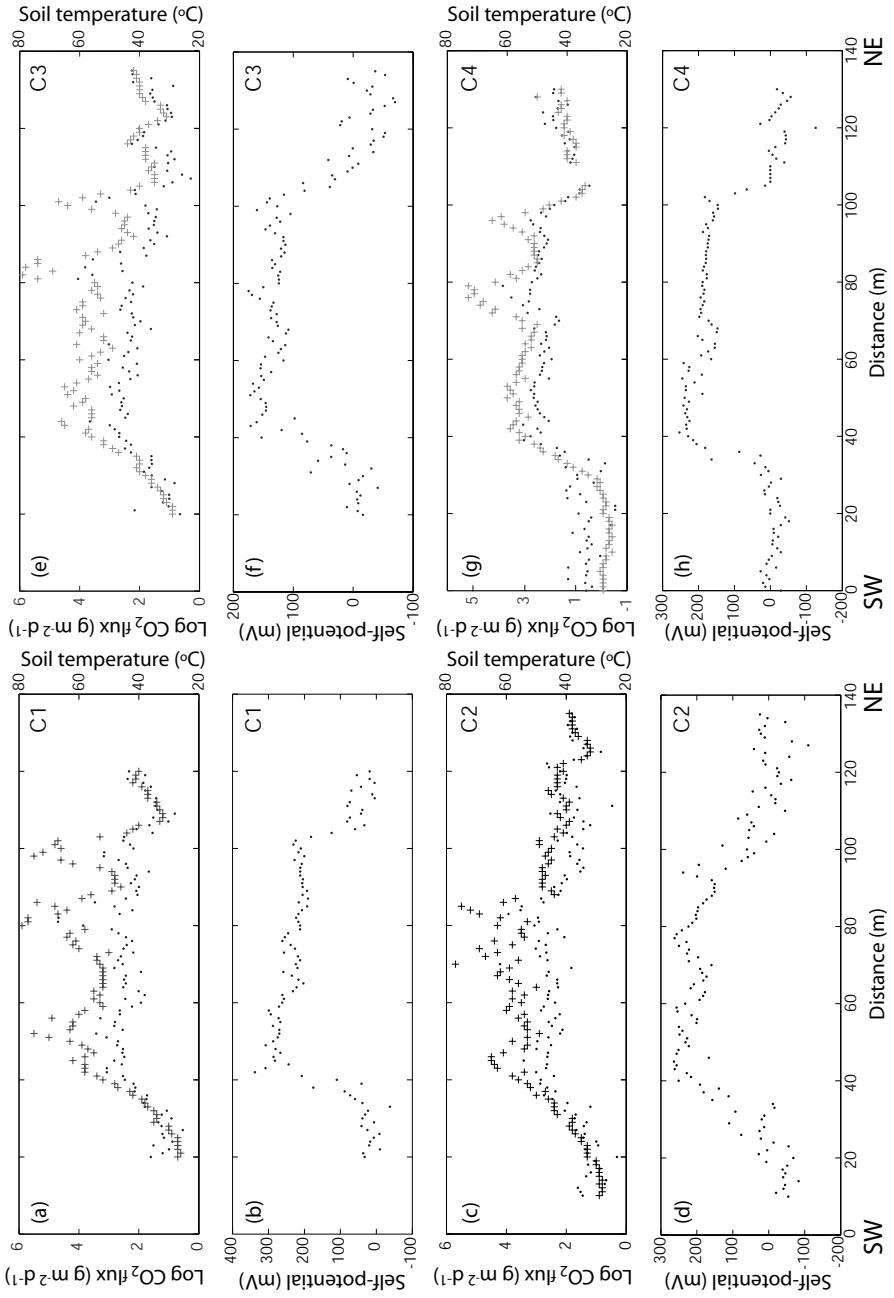

Figure 3. Plots of log CO_2 flux and soil temperature versus distance along transects (a) C1, (c) C2, (e) C3, and (g) C4 (see Figure 2). Dots and pluses are log CO_2 flux and soil temperature, respectively. Plots of SP versus distance along transects (b) C1, (d) C2, (f) C3, and (h) C4.